J. Fluid Mech. (2015), *vol.* 782, R2, doi:10.1017/jfm.2015.560

JFM RAPIDS
journals.cambridge.org/rapids

Viscous fingering and deformation of a miscible circular blob in a rectilinear displacement in porous media

Satyajit Pramanik[1,†], **A. De Wit**[2] **and Manoranjan Mishra**[1]

[1]Department of Mathematics, Indian Institute of Technology Ropar, Rupnagar 140001, India

[2]Université libre de Bruxelles (ULB), Nonlinear Physical Chemistry Unit, CP231, 1050 Brussels, Belgium

(Received 31 July 2015; revised 19 September 2015; accepted 21 September 2015)

The deformation of an initially circular miscible blob in a rectilinear displacement is investigated numerically for porous media when the blob is more viscous than the displacing fluid. We find in the parameter space spanned by the Péclet number and log-mobility ratio the existence of a new lump-shaped instability zone between two distinct regimes of comet and viscous fingering (VF) deformations. The more viscous circular blob is destabilized by VF only over a finite window of log-mobility ratio, contrary to the displacement of a more viscous finite slice with planar interfaces. This difference is attributed to the initial curvature of the miscible blob.

Key words: fingering instability, mixing, porous media

1. Introduction

Understanding displacement and mixing of fluids in porous media (Jha, Cueto-Felgueroso & Juanes 2011*a*; Nicolaides *et al.* 2015) is an active area of research devoted to characterizing industrial and environmental processes, such as oil recovery (Homsy 1987), pollution remediation (Welty, Kane & Kauffman 2003), CO_2 sequestration (Ott, Berg & Oedai 2012; Huppert & Neufeld 2014) and chromatographic separation (De Wit, Bertho & Martin 2005), to name a few. The mixing and dispersion of one fluid within another one can usually be significantly increased by hydrodynamic instabilities such as viscous fingering (VF). VF occurs typically in a porous medium when a fluid of given viscosity displaces a more viscous and hence less mobile one (Homsy 1987; Mishra *et al.* 2010; Jha *et al.* 2011*a*). It deforms the interface into 'fingers', which enhances mixing (Jha *et al.* 2011*a*; Jha, Cueto-Felgueroso & Juanes 2011*b*; Dentz *et al.* 2011; Jha, Cueto-Felgueroso & Juanes 2013) between the two fluids and is usually detrimental to displacement efficiency.

† Email address for correspondence: satyajit.math16@gmail.com

Several articles have been devoted to analysing miscible VF of either a single interface between two semi-infinite regions (Homsy 1987; Tan & Homsy 1988; Pramanik & Mishra 2013, 2015) or a finite-size rectangular plug in a rectilinear displacement (Chen & Wang 2001; De Wit *et al.* 2005; Mishra, Martin & De Wit 2008). However, in numerous cases, a fluid sample of arbitrary initial geometry can be entrained by a carrier fluid of different viscosity and may deform because of dispersion or VF upon displacement (Nicolaides *et al.* 2015). This is the case for instance in localized pollution events in soils where underground flows may entrain either more or less viscous spills of finite spatial extent. Similarly, in CO_2 sequestration techniques, the CO_2 sample migrates as an irregular plume of finite extent within, for instance, water, oil or brine of different viscosity (Lagneau, Pipart & Catalette 2005; Sauzade & Cubaud 2013; Huppert & Neufeld 2014).

Despite the importance of such applications, understanding the influence of fingering instabilities on the effective dispersion of such localized samples of arbitrary shape has not been given much attention. In the case of buoyancy-driven fingering, earlier works have shown deformation of contaminant plumes injected from a point source because of gradients of density (Mainhagu *et al.* 2012). For viscous effects, Chen, Wang & Meiburg (2001) performed numerical simulations of VF of a less viscous circular blob, showing that Korteweg stresses stabilize the fingering instability at its convex interface and help to form a tail at the trailing edge. De Wit & Homsy (1999) showed that an elliptic deformation and no fingering is observed for less viscous circular samples if the blob is too small and also investigated the influence of reactions on the dynamics. Nicolaides *et al.* (2015) investigated the impact of VF and heterogeneity of permeability on fluid mixing of finite-size samples, showing that breakthrough times and mixing efficiency depend on the relative viscosity of the sample. Maes *et al.* (2010) analysed experimentally in a horizontal Hele-Shaw cell the dispersion and miscible VF of an initially circular, more viscous sample within a rectilinear displacement. The unstable viscosity contrast between the sample and the carrier induced the formation of fingers at the rear of the blob and a downstream tail at the frontal part of the initially circular sample (Maes *et al.* 2010). The dynamics of the more viscous samples as well as the effect of the local curvature of the miscible interface on fingering remain, however, poorly explored.

In this context, we investigate here the deformation and spreading of initially circular blobs displaced rectilinearly by a less viscous carrier fluid in porous media. To do so, we numerically integrate Darcy's law for the evolution of flow velocity coupled to a convection–diffusion equation for the concentration of the solute ruling the viscosity of the miscible blob in a range of log-mobility ratios R, Péclet number Pe and initial radius r (equivalently curvature) of the blob. We show that, for more viscous circular blobs, VF at the rear interface is obtained only in a finite window of R above a critical value of Pe and r. We further identify two different dynamical regimes in which either a comet or a lump deformation of blobs is obtained instead of fingering. We characterize quantitatively the spreading of the blob in the different regimes by computing the variance of the sample in time. Our results pave the way to new insights into the influence of hydrodynamic modes in the spreading of samples of arbitrary shape and viscosity in porous media.

2. Mathematical formulation and numerical solution

We consider a circular blob of initial radius r_d and viscosity μ_2 containing a solute in concentration $c = c_2$, which is displaced in a 2D porous medium of length L and

width W at a uniform velocity U along the x-direction by another fluid of viscosity μ_1 in which $c = 0$. Fluids are assumed to be incompressible and neutrally buoyant and the viscosity to depend on concentration following an Arrhenius relation, $\mu(c) = \mu_1 e^{Rc/c_2}$ (Homsy 1987). To be able to explicitly explore the effects of changing the Péclet number Pe and the radius of the blob on the dynamics, we use for non-dimensionalization the characteristic length scale, $L_c = W/16$, and the time scale L_c/U. With this choice of length, the dimensionless radius $r = r_d/L_c$ is unity when $r_d = W/16$, i.e. when the blob is small enough not to be affected by the boundaries. The characteristic pressure, velocity, viscosity and concentration are taken to be $\mu_1 U L_c/\kappa$, U, μ_1 and c_2, respectively. An isotropic fluid dispersion, D, is assumed for simplicity. The related dimensionless equations in a reference frame moving with the velocity U are

$$\boldsymbol{\nabla}\cdot\boldsymbol{u} = 0, \quad \boldsymbol{\nabla}p = -\mu(c)(\boldsymbol{u}+\boldsymbol{i}), \tag{2.1a,b}$$

$$\partial_t c + \boldsymbol{u}\cdot\boldsymbol{\nabla}c = \frac{\nabla^2 c}{Pe}, \tag{2.2}$$

where $\boldsymbol{i}$ is the unit vector in the x-direction, $\boldsymbol{u} = (u, v)$ is the 2D velocity field and $\mu(c) = e^{Rc}$. The dimensionless initial radius $r = r_d/L_c$, the Péclet number $Pe = UL_c/D$ and the log-mobility ratio $R = \ln(\mu_2/\mu_1)$ are the three dimensionless parameters of the problem.

The boundary conditions in the moving frame of reference are $\boldsymbol{u} = (0, 0)$, $\partial_x c = 0$ as $x \to \pm\infty$ along the longitudinal boundaries, while along the transverse boundaries, $\partial_y v = 0$, $\partial_y c = 0$, $\forall x$. The initial distribution of the concentration is $c = 1$ inside the blob, $c = 0$ outside it, and the initial velocity is $\boldsymbol{u}(x, y) = (0, 0)$. The stream function $\psi(x, y, t)$ (such that $u = \partial_y\psi$ and $v = -\partial_x\psi$) form of the governing equations becomes (Pramanik & Mishra 2015)

$$\nabla^2\psi = -R\boldsymbol{\nabla}c\cdot(\boldsymbol{\nabla}\psi + \boldsymbol{j}), \tag{2.3}$$

$$\partial_t c + (\partial_y\psi)(\partial_x c) - (\partial_x\psi)(\partial_y c) = \frac{\nabla^2 c}{Pe}, \tag{2.4}$$

with $\boldsymbol{j}$ is the unit vector in the y-direction. These equations are numerically solved using a pseudo-spectral method (Tan & Homsy 1988; De Wit *et al.* 2005; Mishra *et al.* 2008) in a computational domain of size $L_x \times L_y$ with periodic boundaries in both x and y directions, where $L_x = L/L_c$, $L_y = W/L_c$. In order to ensure that the boundaries do not influence the dynamics of the blob, we choose a large computational domain with the boundaries far away from the blob, such that $L_x/L_y = 2$, $L_y/r \geqslant 32$ in all the simulations shown here. The number of spectral modes chosen for a computational domain of size 32×16 is 4096×2048. Panels in figures 1–3 only show a small fraction of the numerical domain. Unlike the cases of VF around planar interfaces, no initial perturbations are required at the diffusive interface between the blob and the displacing fluid to trigger the instability, as curvature naturally ensures instability via (2.3), due to the fact that $\boldsymbol{\nabla}c$ and $\boldsymbol{\nabla}\psi$ are not collinear at the curved miscible interface. We performed simulations with and without random perturbations along the circumference of the blob and identical results are obtained for both cases. The time step used is $\Delta t = 10^{-4}$. A convergence study of the numerical method ensures that the fingering dynamics are not affected when using smaller time and spatial discretizations. The accuracy and efficiency of the Fourier pseudo-spectral method used have been verified by calculating the total mass of the blob, which shows a maximum 0.001 % relative error.

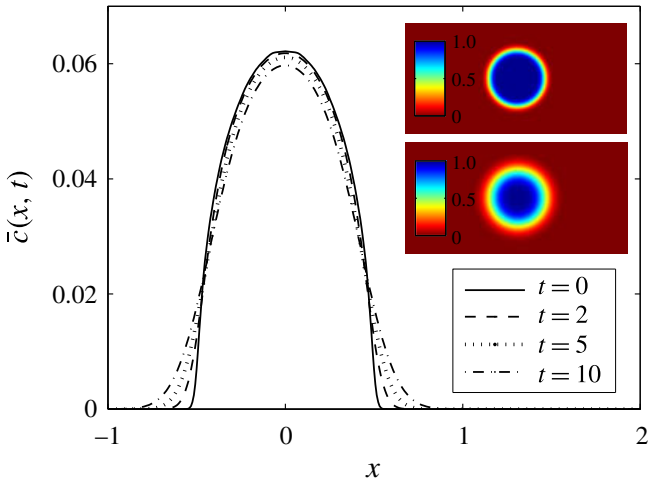

FIGURE 1. Transversely averaged concentration profiles, $\bar{c}(x, t)$, of the blob in the moving reference frame at different times for $R = 0$, $Pe = 1000$, $r = 0.5$. In the absence of viscosity contrast, a diffusive spreading is observed. Inset: spatial distribution of the solute concentration at two different times $t = 2$ and $t = 10$. This depicts that the circular blob diffuses isotropically and simply dilates in the moving frame of reference when the two fluids have the same viscosity.

3. Dynamics of a more viscous miscible blob

First we consider the case where the viscosity of the circular blob is the same as that of the displacing fluid ($R = 0$). The spatial distribution of the solute concentration, $c(x, y, t)$, is shown in the inset of figure 1 in a reference frame moving with the displacing fluid velocity. In this case, the blob diffuses isotropically in all directions and its centre of mass travels at the same velocity as that of the displacing fluid. For such an isotropic dispersion in a porous medium, the one-dimensional averaged distribution of the solute concentration contains all the necessary information: the transversely averaged concentration profiles, $\bar{c}(x, t) = (1/L_y) \int_0^{L_y} c(x, y, t)\, \mathrm{d}y$, feature indeed a diffusive dynamics and keep their radial symmetry in time as seen in figure 1.

How is this symmetric dynamics modified if the sample has a different viscosity than that of the carrier? Here we focus on the $R > 0$ case for which the sample is more viscous than the displacing fluid. Fingering is then expected to develop at the rear part of the blob where the less viscous carrier displaces the more viscous sample (Maes *et al.* 2010). Numerical simulations have been performed in a wide range of r, R and Pe to understand the dynamics of the blob in such flow conditions. Figure 2 depicts the dynamics and $\bar{c}(x, t)$ for $R = 1$, $Pe = 1000$ and two different radii. For both blobs, a downstream tail traces the initial position of the blob. While the sample lags behind the main stream and distorts in time because of fingering for $r = 0.5$, no fingers are seen for $r = 0.25$. This shows the existence for the onset of VF of a critical blob radius, $r_c(R, Pe)$, such that the blob is large enough to feature at least a wavelength of the VF instability at the back interface. The upstream movement of the blob in the moving frame in which the ambient fluid appears stationary can be explained in terms of their relative velocity. Since both fluids flow due to the pressure gradient between the inlet and outlet boundaries of the system, the larger viscosity of the blob results in a slower movement of it in comparison to the surrounding fluid. At the frontal interface, instead of the diffusively stable dynamics as observed for rectangular slices

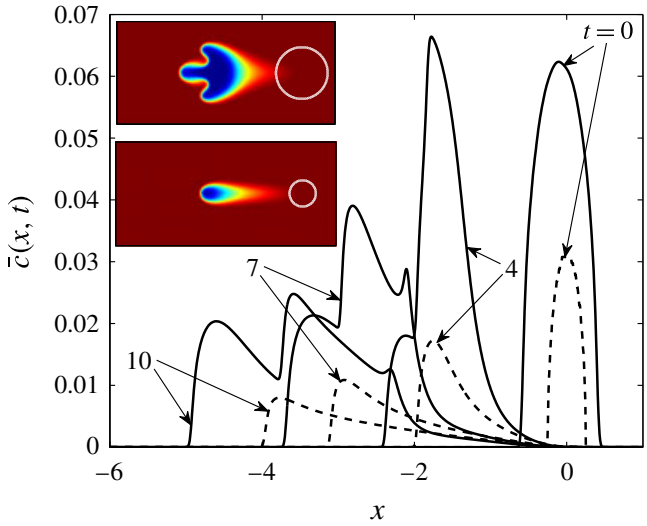

FIGURE 2. Transversely averaged concentration, $\bar{c}(x,t)$, at different times for $R=1$, $Pe=1000$ and $r=0.25$ (dashed line), $r=0.5$ (continuous line). Inset: spatial distribution of the solute concentration at $t=4$ along with the white contour $c=0.01$ of the initial distribution of the blob.

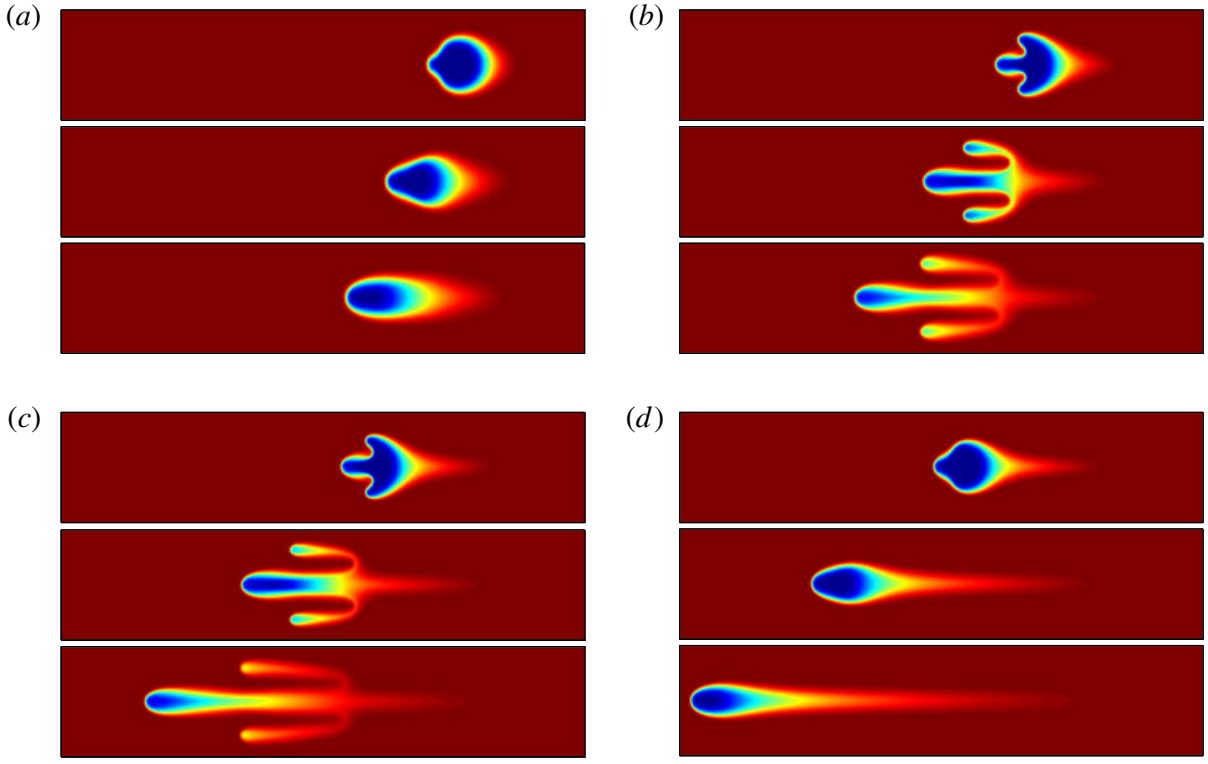

FIGURE 3. Spatial distribution of concentration at $t=4$, 7, 10 from top to bottom for $Pe=1000$, $r=0.5$ and (*a*) $R=0.5$, (*b*) $R=1.0$, (*c*) $R=1.5$ and (*d*) $R=2.0$.

(De Wit *et al.* 2005), the more viscous miscible blob deforms into a diffusive tail to be discussed below.

Figure 3 shows the spatio-temporal evolution of the concentration for different values of $R>0$ for $Pe=1000$ and $r=0.5$. For all R, the dynamics are diffusive and the interface remains almost undeformed at the early stages of the displacement

($t \lesssim 1$). Once viscous effects come into play, a lump is initially formed at the rear interface where the unfavourable viscosity contrast acts. This results in different patterns at later times ($t \gtrsim 4$) depending on the mobility ratio. For $R = 0.5$, the viscous ratio is too small to trigger VF and the blob takes the shape of a comet. Nevertheless, a tendency to finger formation and a transition between slight VF and the comet formation are noticed (figure 3*a*). For $R = 1.0$ and 1.5, the viscous instability becomes dominant and the lump at the rear interface eventually becomes fingered (figure 3*b*,*c*). For a very large viscosity contrast, however, VF is not observed while the sample lags increasingly behind the main flow. As an example, for $R = 2.0$, the lump at the rear interface fails to evolve as VF and the blob ends up as a comet with a long, sharp tail (figure 3*d*). Thus for a fixed *Pe* and *r*, a more viscous miscible blob features VF only for some intermediate viscosity contrast, and it takes the shape of a comet with a downstream tail for other values of $R > 0$. Our simulations reveal that with increasing *R* the blob moves faster in the upstream direction in the moving frame of reference. When mapped to the fixed reference frame, this means that the detachment time of the blob from its initial position increases with *R*, similarly to what is observed in experiments by (Maes *et al.* 2010, see figure 13).

The dynamics and the flow pattern around a blob of given radius are thus determined by the viscosity contrast *R* and *Pe*. To understand this, we recall that, for miscible VF, the wavelength of the most unstable mode decreases when *R* increases (Homsy 1987; Tan & Homsy 1988). Therefore, for given *r* and *Pe*, VF is observed as soon as the VF wavelength fits into the width of the rear unstable interface of the blob. This explains why the blob features fingers for $R = 1.0$ and 1.5 while it does not for $R = 0.5$, for which the wavelength of VF is too large to deform the blob. For planar interfaces, more fingers are observed when *R* is increased from 1.5 to 2.0. In contrast, for the curved miscible blob, when *R* is increased beyond a threshold value that depends on *Pe*, the displacing fluid preferentially flows around the too viscous sample. This suppresses the finger formation at the rear interface of the circular blob. The streamline distribution in the vicinity of the blob helps to visualize this effect more clearly (figure 4).

Interestingly, it is thus observed that, for certain flow conditions, a more viscous blob may not feature any fingering instability at the rear interface, even in the presence of an unfavourable viscosity contrast. Instead, the blob deforms into a comet shape with a downstream tail at the frontal interface, where the viscosity contrast is stable. We summarize in figure 4 the dynamics of a more viscous blob for $r = 0.5$ in the phase plane spanned by *R* and *Pe*. Three different instability regimes are obtained: comet shape (I), lump shape (II) and VF (III). This reveals the existence of a critical Péclet number, Pe_c, and log-mobility ratio, R_c, for the onset of VF for a given *r* (in this case $Pe_c \approx 925$, $R_c \approx 1.25$ for $r = 0.5$). Along constant $Pe > Pe_c$ lines in the phase plane, the blob undergoes a transition from a comet formation to VF instability and then back to a comet shape with increasing *R*. Thus, there exists an *R*-window, $R_c^l(Pe, r) \leqslant R \leqslant R_c^u(Pe, r)$, for the occurrence of VF, the width of which increases with *Pe* with transition zones on both sides. In particular we have $R_c^l \approx 0.75$, $R_c^u \approx 1.75$ for $Pe = 1000$ and $R_c^l \approx 0.53$, $R_c^u \approx 2.0$ for $Pe = 1200$.

The most specific feature of the rectilinear displacement of a more viscous miscible blob is thus the existence of VF over a finite window of *R*, unlike planar interfaces which feature an increased VF instability for any $R > 0$ (Homsy 1987; Tan & Homsy 1988). The curvature of the diffusive interface and the possibility for the displacing fluid to flow around the sample induce this novel dynamics, which, to the best of our knowledge, has not been characterized in earlier studies. Unlike *R*, no finite VF

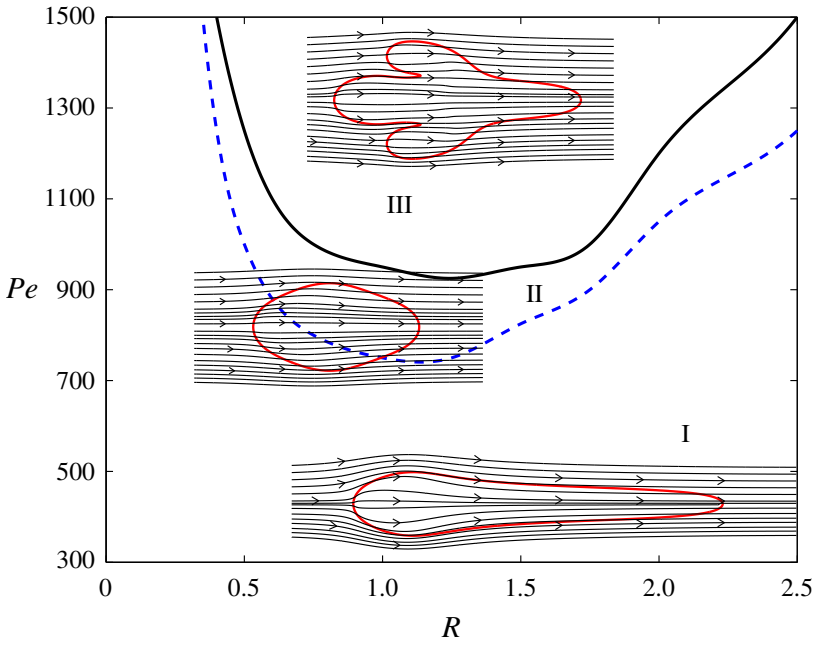

FIGURE 4. Phase plot in the R–Pe plane for $r = 0.5$ showing three distinct instability regimes: comet shape (I), lump shape (II) and VF (III). Streamlines in the vicinity of the blob (contour $c = 0.01$) are presented at $t = 7$ with $Pe = 1000$ for $R = 0.5$, 1.0 and 2.0 in the regions II, III and I, respectively. See supplementary movies 1, 2 and 3 for the animation of the spatio-temporal evolution of a circular blob corresponding to the regions I, II and III, respectively available at http://dx.doi.org/10.1017/jfm.2015.560.

window is obtained for Pe or r. The radius of the blob, r, represents the reciprocal of the curvature of the miscible diffusive interface. In the limit $r \to \infty$, we recover a displacement with a single flat interface, which features VF for any $Pe > Pe_c$ and unstable viscosity contrast, $R > 0$ (Homsy 1987). For a fixed $r > r_c$ and $R = R_c$, the VF instability becomes stronger as Pe increases above Pe_c because increasing the injection speed is known to reinforce the instability.

The streamline distribution in the vicinity of the blob depends on the viscosity contrast. With increasing R, the velocity of the displacing fluid around the blob increases, hence resulting in a longer tail formation, which is readily evident from the streamline distributions (figure 4). In the present study, both the viscosity and the relative velocity between the ambient fluid and the miscible blob increase with R. It is observed that the length of the tail of the comet increases with R. It will be interesting in the future to consider effects of inertia on the dynamics of a miscible blob using the inertia-corrected Darcy law for Hele-Shaw cells (Ruyer-Quil 2001) or the Navier–Stokes equations (Talon, Goyal & Meiburg 2013).

To investigate the efficiency of mixing in the overall dynamics of the displacement we analyse the temporal evolution of the variance (Mishra *et al.* 2008),

$$\sigma_x^2(t) = \frac{\displaystyle\int_0^{L_x} x^2 \bar{c}(x,t)\,\mathrm{d}x}{\displaystyle\int_0^{L_x} \bar{c}(x,t)\,\mathrm{d}x} - \left(\frac{\displaystyle\int_0^{L_x} x \bar{c}(x,t)\,\mathrm{d}x}{\displaystyle\int_0^{L_x} \bar{c}(x,t)\,\mathrm{d}x} \right)^2, \tag{3.1}$$

of $\bar{c}(x, t)$, for different R and Pe. For VF at a planar interface, the variance, σ_x^2, is linear in time in the diffusion-dominated regime (i.e. $\sigma_x^2 \sim t$), while in the

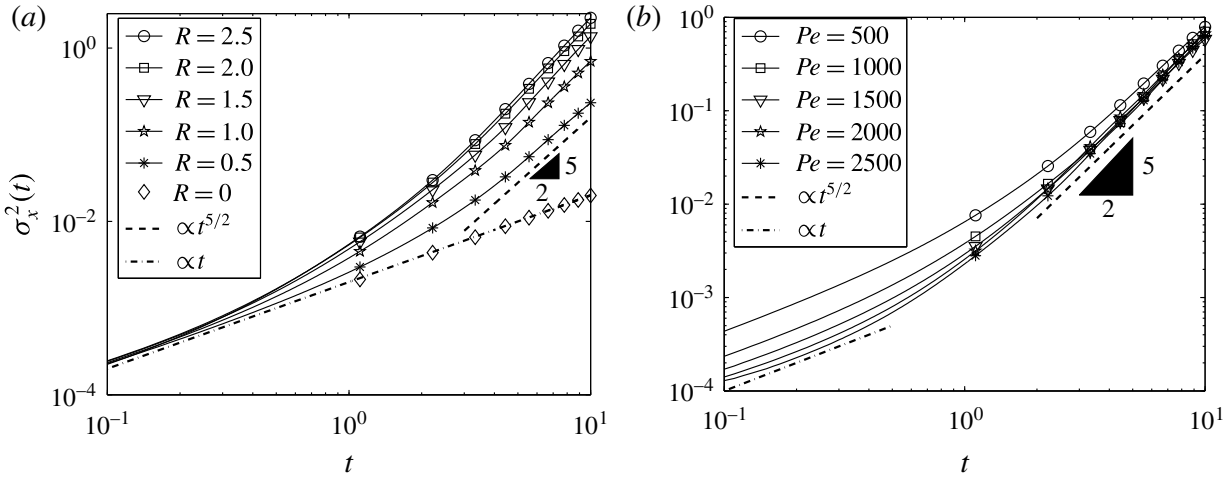

FIGURE 5. Temporal evolution of the axial variance, $\sigma_x^2(t)$, for $r = 0.5$: (*a*) effect of R, (*b*) effect of Pe. In the early diffusive regime, the variance increases linearly with time. At a fixed time, $\sigma_x^2(t)$ is then almost independent of $R \neq 0$ while it decreases when Pe increases. In the later convective regime, $\sigma_x^2(t)$ grows as $t^{5/2}$, i.e. there is enhanced spreading due to the tail formed downstream. The variance then also depends nonlinearly on R while it does not change much when Pe is varied.

convection-dominated VF regime $\sigma_x^2 \sim t^2$ (Tan & Homsy 1988). Here we investigate how the interface curvature and flow past the miscible blob change the variance of the transversely averaged concentration profile. Figure 5(*a*) shows that, for a blob of radius $r = 0.5$ and constant Pe, $\sigma_x^2(t)$ grows indeed linearly in the diffusion-dominated regime ($t \lesssim 0.5$). Afterwards, the variance grows at a higher rate than linear in time and finally tends to follow a power law, $\sigma_x^2(t) \sim t^{5/2}$ at a later time $t \gtrsim 3$. This power-law dependence turns out to be almost independent of the viscosity contrasts considered here as seen in figure 5(*a*). It seems thus that the tail formed by the flow of the displacing fluid around the curved blob enhances the spreading of the finite solute with regard to VF of a planar interface. For $R = 1.0$ and 1.5 this spreading is a combination of VF and downstream tailing, while for the other values of R it is only due to the tail formation. This reflects the fact that the overall spreading is enhanced by the tailing phenomenon, which has a weak dependence on the log-mobility ratio R. The dependence on Pe of the axial spreading shown in figure 5(*b*) exhibits the same temporal evolution of $\sigma_x^2(t)$ in the diffusive and convective regimes as in figure 5(*a*). This shows that, in the convection-dominated regime, enhanced spreading is almost independent of the Péclet number Pe.

4. Conclusion

We have numerically studied the dynamics of more viscous circular blobs when displaced rectilinearly by a less viscous miscible fluid in a homogeneous porous medium. The stability of the rear interface of the curved blob with regard to VF has been studied in the parameter space spanned by the initial radius r of the circular sample, the log-mobility ratio R and the Péclet number Pe. We find that the curvature of the blob induces new dynamics when the viscosity contrast is large enough. Indeed, we showed that VF develops at the rear interface of large enough blobs only over a finite window of R when $Pe > Pe_c$. Outside it, comet and lump-shaped deformations of the blob are obtained. This is due to the fact that, for too small blobs, the width of

the rear interface is too small to accommodate a VF wavelength. On the other hand, for larger blobs and above a given R, the displacing fluid prefers to flow around the finite-size viscous sample rather than to destabilize its rear.

This is in strong contrast with what happens for planar interfaces recovered for $r \to \infty$ that feature VF for any $R > 0$. The present numerical simulations agree qualitatively with the experimental observation by Maes *et al.* (2010) of fingering and tail formation in the rectilinear displacement in Hele-Shaw cells of more viscous circular blobs. We further show that the presence of a tail behind the sample in the comet shape dynamics induces enhanced mixing with the variance of the sample increasing as $t^{5/2}$.

Our results thus show that the curvature of finite-size samples is of importance as different viscously driven dynamics (lump and comet formation with a finite R-window for VF instability) are obtained with regard to the planar interface case. This is of importance when quantifying the characteristics of mixing of finite-size plumes in soils and should guide further experiments devoted to analysing such mixing dynamics. Preliminary results show that the existence of a finite R-window for VF is also obtained for an initially squared blob. It will be interesting to analyse in future works whether the squared shape can also induce other instability modes. Analysis of the effects of velocity-dependent dispersion (Bacri, Salin & Wouméni 1991) and inertia (Talon *et al.* 2013) has also been undertaken.

Acknowledgements

S.P. gratefully thanks the National Board for Higher Mathematics, Department of Atomic Energy, Government of India for the financial support through a PhD fellowship. He also thanks Professor H. C. Kuhlmann for hosting at TU Wien as an Ernst Mach scholar of OeAD (Austria) during the preparation of the manuscript. A.D. acknowledges financial support of PRODEX and of the FRS-FNRS FORECAST project.

Supplementary movies

Supplementary movies are available at http://dx.doi.org/10.1017/jfm.2015.560.

References

Bacri, J.-C., Salin, D. & Wouméni, R. 1991 Three dimensional miscible viscous fingering in porous media. *Phys. Rev. Lett.* **67**, 2005–2008.

Chen, C.-Y., Wang, L. & Meiburg, E. 2001 Miscible droplet in a porous medium and the effects of Korteweg stresses. *Phys. Fluids* **13** (9), 2447–2456.

Chen, C.-Y. & Wang, S.-W. 2001 Miscible displacement of a layer with finite width in porous media. *Intl J. Numer. Meth. Heat Fluid Flow* **11**, 761–778.

Dentz, M., Le Borgne, T., Englert, A. & Bijeljic, B. 2011 Mixing, spreading and reaction in heterogeneous media: a brief review. *J. Contam. Hydrol.* **120–121**, 1–21.

De Wit, A. & Homsy, G. M. 1999 Viscous fingering in reaction–diffusion systems. *J. Chem. Phys.* **110**, 8663–8675.

De Wit, A., Bertho, Y. & Martin, M. 2005 Viscous fingering of miscible slices. *Phys. Fluids* **17**, 054114.

Homsy, G. M. 1987 Viscous fingering in porous media. *Annu. Rev. Fluid Mech.* **19**, 271–311.

Huppert, H. E. & Neufeld, J. A. 2014 The fluid mechanics of carbon dioxide sequestration. *Annu. Rev. Fluid Mech.* **46**, 255–272.

Jha, B., Cueto-Felgueroso, L. & Juanes, R. 2011*a* Fluid mixing from viscous fingering. *Phys. Rev. Lett.* **106**, 194502.

JHA, B., CUETO-FELGUEROSO, L. & JUANES, R. 2011*b* Quantifying mixing in viscously unstable porous media flows. *Phys. Rev.* E **84**, 066312.

JHA, B., CUETO-FELGUEROSO, L. & JUANES, R. 2013 Synergetic fluid mixing from viscous fingering and alternating injection. *Phys. Rev. Lett.* **111**, 144501.

LAGNEAU, V., PIPART, A. & CATALETTE, H. 2005 Reactive transport modelling of CO_2 sequestration in deep saline aquifers. *Oil Gas Sci. Technol.* **60** (2), 231–247.

MAES, R., ROUSSEAUX, G., SCHEID, B., MISHRA, M., COLINET, P. & DE WIT, A. 2010 Experimental study of dispersion and miscible viscous fingering of initially circular samples in Hele-Shaw cells. *Phys. Fluids* **22**, 123104.

MAINHAGU, J., GOLFIER, F., OLTÉAN, C. & BUÈS, M. A. 2012 Gravity-driven fingers in fractures: experimental study and dispersion analysis by moment method for a point-source injection. *J. Contam. Hydrol.* **132**, 12–27.

MISHRA, M., MARTIN, M. & DE WIT, A. 2008 Differences in miscible viscous fingering of finite width slices with positive or negative log mobility ratio. *Phys. Rev.* E **78**, 066306.

MISHRA, M., TREVELYAN, P. M. J., ALMARCHA, C. & DE WIT, A. 2010 Influence of double diffusive effects on miscible viscous fingering. *Phys. Rev. Lett.* **105**, 204501.

NICOLAIDES, C., JHA, B., CUETO-FELGUEROSO, L. & JUANES, R. 2015 Impact of viscous fingering and permeability heterogeneity on fluid mixing in porous media. *Water Resour. Res.* **51**, 2634–2647.

OTT, H., BERG, S. & OEDAI, S. 2012 Displacement and mass transfer of CO_2/brine in sandstone. *Energy Procedia* **23**, 512–520.

PRAMANIK, S. & MISHRA, M. 2013 Linear stability analysis of Korteweg stresses effect on miscible viscous fingering in porous media. *Phys. Fluids* **25**, 0741404.

PRAMANIK, S. & MISHRA, M. 2015 Effect of Péclet number on miscible rectilinear displacement in a Hele-Shaw cell. *Phys. Rev.* E **91**, 033006.

RUYER-QUIL, C. 2001 Inertial corrections to the Darcy law in a Hele-Shaw cell. *C. R. Acad. Sci. IIb Mech.* **329**, 337–342.

SAUZADE, M. & CUBAUD, T. 2013 Initial microfluidic dissolution regime of CO_2 bubbles in viscous oils. *Phys. Rev.* E **88**, 051001(R).

TALON, L., GOYAL, N. & MEIBURG, E. 2013 Variable density and viscosity, miscible displacements in Hele-Shaw cells. Part 1. Linear stability analysis. *J. Fluid Mech.* **721**, 268–294.

TAN, C. T. & HOMSY, G. M. 1988 Simulation of non-linear viscous fingering in miscible displacement. *Phys. Fluids* **31**, 1330.

WELTY, C., KANE, A. C. III & KAUFFMAN, L. J. 2003 Stochastic analysis of transverse dispersion in density-coupled transport in aquifers. *Water Resour. Res.* **39**, 1150.